Multidisciplinary Materials Chronicles, 2025, Vol. 2, Iss. 1, 104-111

DOI: 10.62184/mmc.jmmc110020255

Research Article

SCIENCE PARK PUBLISHER

Multidisciplinary Materials Chronicles

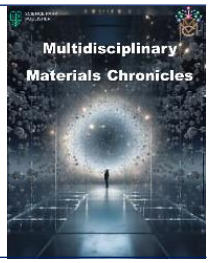

The effect of TeO_2, ZnO, and NiO ratios in enhancing the radiation shielding, structural, and mechanical features of the provided glass sample

Roya Boudaghi Malidarreh*

Institute of Physics and Technology, Ural Federal University, Yekaterinburg, Russia

Received: 16, 02, 2025; Accepted: 10, 04, 2025; Published: 04, 06, 2025

Abstract

This paper focuses on the radiation shielding, structural, and mechanical properties of the Te glass system using the FLUKA Monte Carlo (MC) environment and Phy-X: PSD software. In this work, three selected glass specimens with the formula of TeO_2+ZnO+xNiO, where x=4,8 and 12 mol.%, NiO have been used. This study assessed the key radiation metrics such as Half Value Layer (HVL) and Effective Atomic Number (Z_{eff}) for wide energy ranges. The results show a clear relationship between increased NiO concentration and gamma photon shielding performance in the provided specimens. Furthermore, micro-Hardness (H) and poisson's ratio σ have been improved. Moreover, findings reveal that increasing the density gives rise to the V_t, while the inverse trend is mirrored in G_t values. The outcomes of the present work are suitable for future studies related to the novel Te glass series. The findings highlight the effectiveness of Te-enriched glass specimens in terms of radiation shielding.

Keywords: FLUKA MC Environment, Te-enriched Glass Specimens, HVL, Mechanical Moduli

1. Introduction

The quest for development in all fields of medicine, radiation therapy, nuclear engineering, and quality control requires the development of innovative and novel instruments and modalities [1-3]. These instruments utilize both charged and uncharged particles to irradiate materials/products or tissues for specific clinical and industrial purposes. As a result, they may cause injuries in organs and lead to secondary cancer risk [2, 4]. On the other hand, minimizing the range of received doses by organs prevents injuries and cancer risks, thereby highlighting the significance of effective radiation protection techniques [5-7]. Thus, understanding the concept of interactions of radiation with materials became essential. At this stage, gamma photons, known for their high penetrating ability and lack of charge, emerge as the primary concern in radiation protection. This has attracted considerable attention in recent times [6, 8]. Although traditional materials like concrete and lead have been extensively discussed in many literatures, they possess several disadvantages, including toxicity, opacity, and a limited range of applications, which restrict their use to specific contexts [9-11]. In contrast, glass has emerged as a more effective material, offering a wider range of applications [12-16].

Tellurium (Te) is related to group 16 in the periodic table. This element is a positive material for gamma photon radiation applications. This element has attracted significant attention from developers of radiation shielding materials in the form of glass in clinical trials and industry [17-19]. Te is toxic and widely utilized in pharmaceutical technology in nano form [20]. Findings show that incorporating specific chemical compositions can enhance the radiation shielding performance of Te glass types. Although the effects of Zinc Oxide (ZnO) and Nickel Oxide (NiO) have been explored in several studies [21-

Multidisciplinary Materials Chronicles, 2025, Vol. 2, Iss. 1, 104-111
DOI: 10.62184/mmc.jmmc110020255

Research Article

23], few have examined the impact of additives on the mechanical properties, which is the aim of the present work. Hence, this work delves into radiation shielding and mechanical features of the provided glass specimens, formulated as TeO_2+ZnO+NiO, and designated as 4:1-xNiO with x varying from 4 to 12 mol.% NiO. The study employs the FLUKA MC simulation framework and the Makishima and Mackenzie (MM) model.

2. Methodologies

2.1. Glass samples' characteristics

The present work investigates novel glass radiation shielding performance leveraging the FLUKA MC code according to Table 1. The glass specification, molar volume, and density have been listed in **Table 1**. In addition, a graphical representation of the glass compositions (in mol.%) is represented in **Figure 1**.

Table 1. The specifications of the provided glass specimens.

specimens	Molar volume ($cm^3.mol^{-1}$)	Density ($g.cm^{-3}$)
4:1-4.0NiO	25.49	5.70
4:1-8.0NiO	24.94	5.74
4:1-12NiO	24.40	5.78

2.2. FLUKA simulation study

Different materials' performance in terms of radiation shielding has garnered increasing attention in recent research. The high precision of the Monte Carlo (MC) methodology demonstrated in prior studies, especially concerning radiation shielding, highlights the necessity of applying the MC approach for further investigations. Consequently, this study evaluates the efficacy of a specific Te-enriched glass system using the MC technique FLUKA [24].

The simulation input file includes geometry details such as source, glass samples, lead collimator, NaI detector, and the compositions of each cell. The entire system is enclosed within a black-hole region, ensuring that no particles are tracked beyond this boundary. The study involved irradiating three provided glass specimens with several simulated mono-energetic photon sources. Key cards used in this study include BEAM, BEAMPOS, MATERIAL, COMPOUND, USRBDX, USRBIN scoring cards, and geometry cards. The BEAM and BEAMPOS cards define the characteristics of the radiation, while the geometry cards facilitate the simulation of complex geometries using the FLUKA code and Flair environment. Each cell in geometry is assigned specific materials through the MATERIAL and COMPOUND cards. The USRBDX and USRBIN scoring cards enable tracking and recording of particles when they reach the detector. The study defined 10^7 primary events over five cycles to derive the data. **Figure 2 (a, b)** illustrates the 2-D and 3-D schematics of the MC simulation.

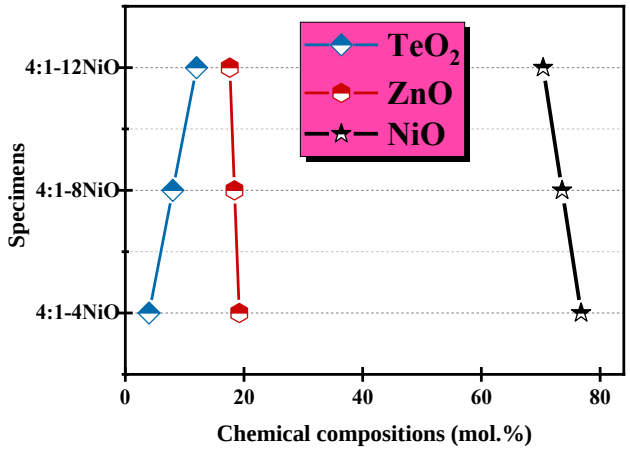

Figure 1. Graphical representation of the chemical compositions (in mol.%) for provided specimens.

Multidisciplinary Materials Chronicles, 2025, Vol. 2, Iss. 1, 104-111

DOI: 10.62184/mmc.jmmc110020255

Research Article

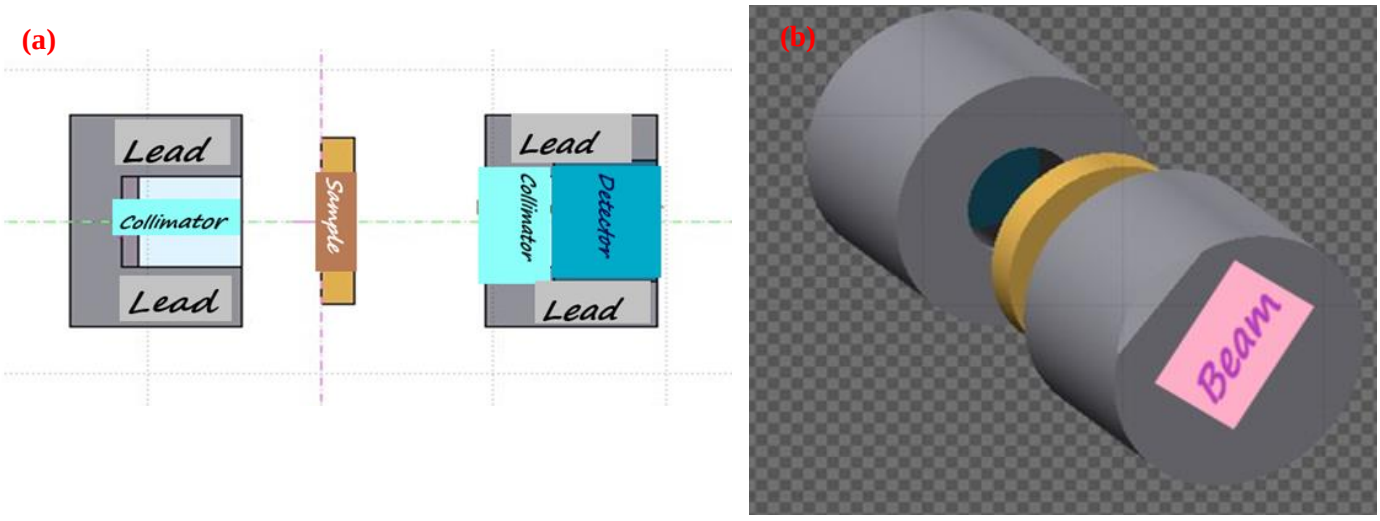

Figure 2. (a) 2-D and **(b)** 3-D FLUKA simulation of the provided ternary glass samples.

2.3. Radiation shielding features

The attenuation parameter, like the Half value layer (HVL), is extracted based on the Linear attenuation coefficient (LAC) and Beer-Lambert's law by Equations 1-2 [25, 26]:

$$LAC\ (cm^{-1}) = \frac{1}{x} Ln(\frac{I_0}{I}) \qquad (1)$$

Where I_0 and I are unattenuated and attenuated gamma photons. x is the thickness of the samples.

$$HVL(cm) = \frac{Ln(2)}{LAC\ (cm^{-1})} \qquad (2)$$

The Effective atomic number (Z_{eff}) is crucial in assessing the shielding capabilities of selected samples, as determined using the Phy-X: PSD code. Phy-X: PSD is an accessible and user-friendly software that enables the analysis of attenuation properties in composites, glasses, and other materials. These factors can be evaluated by entering their weight percentage (wt.%), mole percentage (mol%), and density. This tool is readily available for researchers at https://phy-x.net/ [27].

2.4. Structural and mechanical properties utilizing MM model

The MM model [28, 29] is a superior factor in estimating the mechanical features, which is our concern in this section. Accordingly, they were determined using the formulas provided in Equations 6-11 based on bond dissociation energy (G_t), packing factor (V_i), and packing density (V_t) (see Equations 3-5). These mechanical factors are Young's (Y), bulk (B), shear (S), longitudinal (L) moduli, micro-hardness (H), and Poisson's ratio (σ).

$$G_t\left(\frac{kJ}{cm^3}\right) = \sum_i G_i x_i \qquad (3)$$

$$V_i\left(\frac{cm^3}{mol}\right) = \frac{4\pi}{3} N_A\left(xR_A^3 + yR_o^3\right) \qquad (4)$$

$$V_t\left(\frac{cm^3}{mol}\right) = \frac{\rho}{M}\sum_i V_i x_i \qquad (5)$$

$$Y\ (GPa) = 8.36 V_t G_t \qquad (6)$$

$$B(GPa) = 10 V_t^2 G_t \qquad (7)$$

$$S(GPa) = \frac{30 V_t^2 G_t}{(10.2 V_t - 1)} \qquad (8)$$

$$L(GPa) = B + \frac{4}{3} S \qquad (9)$$

$$\sigma = 0.5 - \frac{1}{7.2 V_t} \qquad (10)$$

$$H = (\frac{1 - 2\sigma}{6(1 + \sigma)}) Y \qquad (11)$$

Where N_A, R_A^3, R_o^3, x, and y represent Avogadro's number, ionic radius of the metal, ionic radius of oxygen, the number of metal atoms, and the number of oxygen atoms, respectively [29-31].

Multidisciplinary Materials Chronicles, 2025, Vol. 2, Iss. 1, 104-111

DOI: 10.62184/mmc.jmmc110020255

Research Article

3. Results and discussion

Figures 3 and 4 show the simulated gamma photon distributions as fluence for ^{137}Cs and ^{60}Co sources, respectively, highlighting distinct peaks at the corresponding energies of 0.662, 1.173, and 1.332 MeV. As anticipated, the gamma photon peaks were highest in the without sample case (in the air-unattenuated spectrum). However, in the presence of the 4:1-4NiO ternary sample (attenuated spectrum), the spectrum exhibited its lowest values, demonstrating the effectiveness of gamma photon shielding performance. Additionally, when samples are irradiated by ^{137}Cs and ^{60}Co, wider and broader peaks are observed in comparison to air case which is due to the gamma photon interactions with the glass samples.

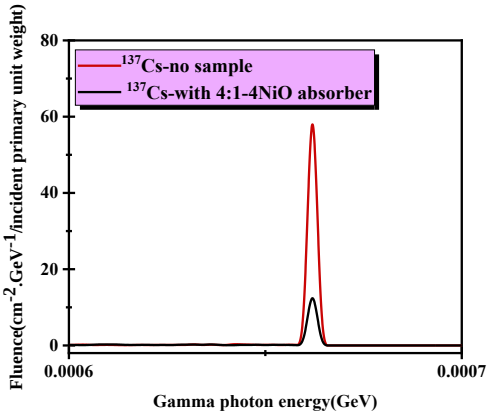

Figure 3. Attenuated and unattenuated gamma photon fluence by ^{137}Cs irradiation.

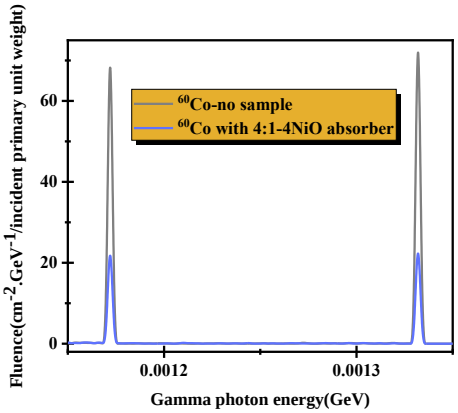

Figure 4. Attenuated and unattenuated gamma photon fluence by ^{60}Co irradiation.

The shielding performance of the glass samples can be gauged by HVL. Thus, the HVL values of the prepared novel glass have been extracted and revealed in **Figure 5.** Generally, the lower values of HVL typically translate to more effective radiation shielding. As anticipated, increasing the NiO contents in the glass system increases the gamma photon shielding efficiency, likely due to the corresponding increase in density values. All series exhibit a similar trend across wide energy ranges, with the dominance of PhotoElectric (P-E), Compton Scattering (C-S), and Pair Production (P-P) processes in various energy zones [17]. In the low energy region, the HVL values are relatively similar, whereas in the high energy range, they show greater divergence. For instance, HVL values for provided glasses vary between 0.002 and 3.284 cm, 0.002 and 3.274 cm, 0.002 and 3.266 cm, ranging from 0.015 to 10 MeV for 4:1-4, 4:1-8 4:1-12 specimens. Although HVL results show compliance specifically in low energy ranges, 4:1-12NiO has the lowest HVL and shows the best gamma photon shielding performance. Hence, there is a linear relationship between increased NiO content and HVL values. Since the energy and chemical composition of each glass sample are effective in the HVL behavior, in this specific glass sample, the chemical composition is less effective in comparison with the energy range.

Figure 6 graphically articulates the Z_{eff} values spanning from 0.015 to 15 MeV using the Phy-X: PSD software for Te novel glass system. A sharp fall and a smooth increase have been recorded for wide energy zones. A detailed analysis of the presented data shows that the Z_{eff} is proportional to Z^{-1}, Z, and Z^2 because of gamma photon interaction in different energy ranges [13]. A Z_{eff} profile reveals that this factor is energy dependent, specifically in low-energy regions, and only in certain high-energy ranges they show effectiveness against chemical compositions. Z_{eff} values show a graduation from 31.95 for 4:1-4NiO to 31.37 for 4:1-12NiO at 15 MeV energy range. Concurrently, a decrease in the contents of TeO_2 and ZnO indicates a complex interaction probability with radiation and highlights the attenuation concept. Hence, the 4:1-4NiO glass specimens, characterized by the highest concentrations of TeO_2 and ZnO and the lowest concentration of NiO, exhibit the highest Z_{eff}, particularly in high-energy regions.

The structural and mechanical parameters of the Te glass system have been obtained through MM model for oxide glasses using the analytical method (**See Figures 7-9)**. The G_t and V_t against density have been represented for the provided glass specimens in **Figure 7.**

Multidisciplinary Materials Chronicles, 2025, Vol. 2, Iss. 1, 104-111

DOI: 10.62184/mmc.jmmc110020255

Research Article

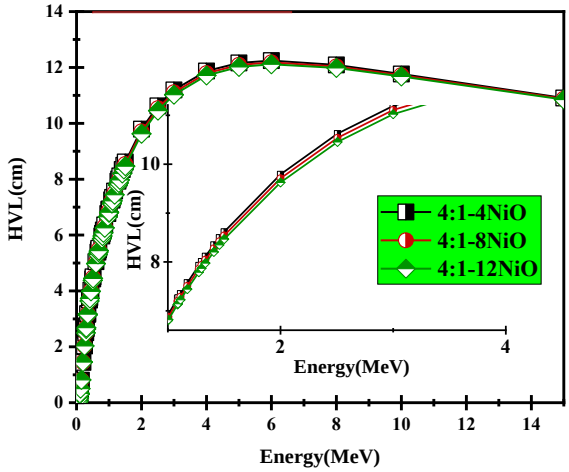

Figure 5. HVL values obtained for glass system.

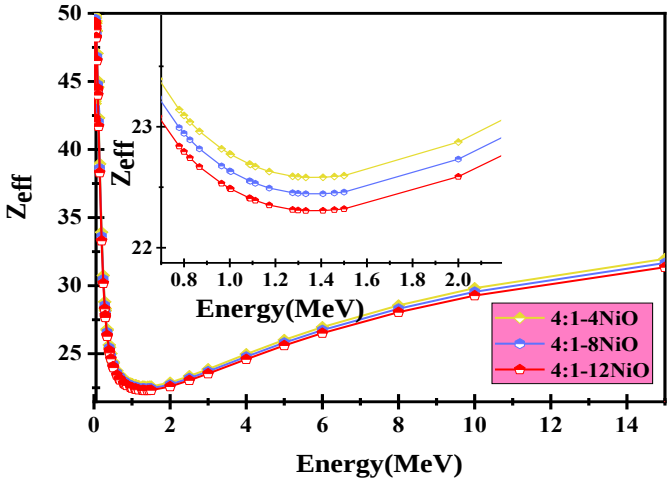

Figure 6. Z_{eff} values obtained for Te glass system ranging from 0.015 to 10 MeV.

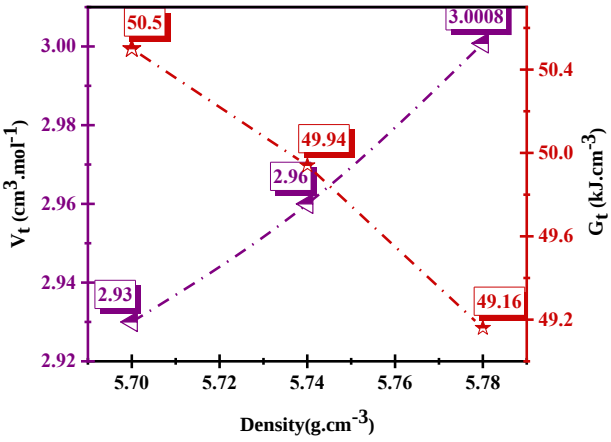

Figure 7. V_t and G_t against density for the provided glass specimens.

Multidisciplinary Materials Chronicles, 2025, Vol. 2, Iss. 1, 104-111

DOI: 10.62184/mmc.jmmc110020255

Research Article

Increasing the density, due to the increment of the NiO mol%, enhances the V_t, while the inverse trend is mirrored for G_t. The V_t values range from 2.93 $\frac{cm^3}{mol}$to 3.0008 $\frac{cm^3}{mol}$ for 4 - 12 mol% NiO, respectively. Meanwhile, the G_t changes from 50.5 $\frac{kJ}{cm^3}$ to 49.16 $\frac{kJ}{cm^3}$ due to the substitution of the TeO_2 and ZnO with NiO. The G_t values for TeO_2 and ZnO are 54 $\frac{kJ}{cm^3}$, 41.5 $\frac{kJ}{cm^3}$, while the value for NiO is 32$\frac{kJ}{cm^3}$. Furthermore, as shown in **Figure 8,** increasing the NiO mol% will decrease the B and L moduli while giving rise to the E and S. For example, the E, B, S, and L for Te:Zn-4NiO are about 1236.987 GPa,4335.375 GPa, 450.257 GPa, and 4920.709 GPa, while these values for 12 mol.% NiO reach about 1233.262, 44426.76, 448.5345, 5009.855 GPa. The calculated H which defines the deformation of the glass network and σ in **Figure 9** show a sharp rise for both parameters by increasing the NiO concentration. It weakens the stiffness of the glass network. In conclusion, our attempts to demonstrate enhancements in the mechanical characteristics of the novel Te glass were unsuccessful. The outcomes exhibited an unstable trend, with minor deviations in the measured properties. Furthermore, a detailed analysis revealed that density is not the sole factor influencing the mechanical characteristics as seen in **Table 1**. From Table 1 and the obtained results can be found that 4:1-12 NiO sample possesses the highest density and is not suitable for mechanical applications.

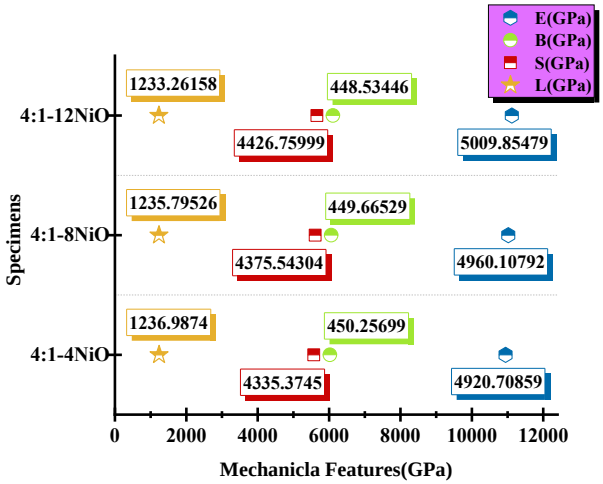

Figure 8. Mechanical moduli for the provided ternary specimens.

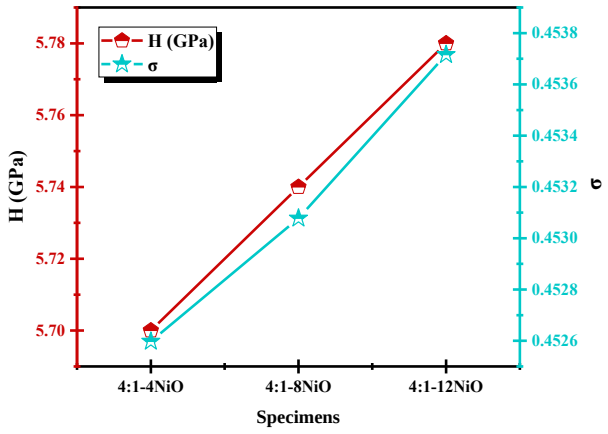

Figure 9. H of the provided ternary specimens, and σ for the provided ternary specimens.

DOI: 10.62184/mmc.jmmc110020255

Research Article

4. Conclusion

The radiation shielding performance of the chosen glass system has been investigated using the FLUKA MC approach. The most important finding in this work was that NiO is a positive material to improve the radiation shielding quality. In addition, increased NiO contents in the glass series reduced the HVL values. They lie from 0.002 cm to 3.284 cm, 0.002 cm to 3.274 cm, and 0.002 cm to 3.266 cm for 4:1-4, 4:1-8, and 4:1-12 specimens. Furthermore, Zeff is directly proportional to Z-1, Z, and Z2. This is because of gamma photons' various mechanisms in different energy ranges. No definite trend has been reported for E, B, S, and L moduli, while we were successful in increasing the H and σ by increasing the NiO mol%. H and σ vary from 5.7 GPa to 5.78 GPa and 0.4526 GPa to 0.45372 GPa for 4-12 mol.% NiO. Hence, our attempts to improve the mechanical qualities were not successful. These findings would open a new path to prepare a new glass system for radiation protection and highlight the effectiveness of Te-enriched glass specimens in terms of radiation shielding.

Author information

Corresponding author: Roya Boudaghi Malidarreh*

E-mail: r.boodaghi66@gmail.com

ORCID iD: 0000-0003-4505-7900

References

[1] R. Khabaz, R. Boodaghi, M.R. Benam, V. Zanganeh, Estimation of photoneutron dosimetric characteristics in tissues/organs using an improved simple model of linac head, J. Appl. Radiat. Isot. 133 (2018) 88-94. https://doi.org/10.1016/j.apradiso.2017.12.023.

[2] S.M. Hosseini Pooya, M.R. Dashtipour, R. Paydar, F. Mianji, B. Pourshahab, A comprehensive dose assessment of irradiated hand by iridium-192 source in industrial radiography, JAPESM, 40 (2017) 611-616. https://doi.org/10.1007/s13246-017-0568-9.

[3] F. Garcia Yip, T. Schneider, M. Reginatto, R. Behrens, L. Buermann, F. Grote, Characterization of small active detectors for electronic brachytherapy dosimetry, JINST, 17 (2022) 3001. https://doi.org/10.1088/1748-0221/17/03/P03001.

[4] R. Khabaz, Phantom dosimetry and cancer risks estimation undergoing 6 MV photon beam by an Elekta SL-25 linac, Appl. Radiat. Isot. 163 (2020) 109232. https://doi.org/10.1016/j.apradiso.2020.109232.

[5] A.S. Abouhaswa, H.M.H. Zakaly, S.A.M. Issa, M. Rashad, M. Pyshkin, H.O. Tekin, R. El-Mallawany, Y.A.M. Mostafa, Synthesis, physical, optical, mechanical, and radiation attenuation properties of TiO_2–Na_2O–Bi_2O_3–B_2O_3 glasses, J. Ceram. Int. 47 (2021) 185–204. https://doi.org/10.1016/j.ceramint.2020.08.122.

[6] A. Sengul, N. Karpuz, I. Akkurt, I. Atik, R. Boodaghi Malidarre, M.I. Sayyed, S. Arslankaya, Computation of the impact of NiO on physical and mechanical properties for lithium nickel phosphate glasses, J. Radiat. Res. Appl. Sc. 16 (2023) 100737. https://doi.org/10.1016/j.jrras.2023.100737.

[7] N. Kutu, Neutron shielding properties of cellulose acetate CdO-ZnO polymer composites, IJCESEN, IJCESEN, 10 (2024) 203. https://doi.org/10.22399/ijcesen.322.

[8] M. Ahmadi, V. Zanganeh, R.B. Malidarre, I. Akkurt, Radiation shielding, physical, and elastic properties of BaO-B_2O_3-Bi_2O_3 glass system, J. Phys. Scr. 97 (2022) 105309. https://doi.org/10.1088/1402-4896/ac9275.

[9] I. Akkurt, H. Akyıldırım, B. Mavi, S. Kilincarslan, C. Basyigit, Photon attenuation coefficients of concrete include barite at different rate, J. Ann. Nucl. Energy. 37 (2010) 910-914. https://doi.org/10.1016/j.anucene.2010.04.001.

[10] W. Gong, H. Yu, H. Ma, N. Wang, L. He, Study on the basic performance of basic magnesium sulfate cement concrete, J. Emerg. Mater. Res. 9 (2020) 618-627. https://doi.org/10.1680/jemmr.19.00039.

[11] M.A.H. Abdullah, R.S.M. Rashid, M. Amran, F. Hejazii, N. M. Azreen, R. Fediuk, Y.L. Voo, N. I. Vatin, M. I. Idris, Recent trends in advanced radiation shielding concrete for construction of facilities: materials and properties, J. Polymers (Basel), 14 (2022) 2830. https://doi.org/10.3390/polym14142830.

[12] R.B. Malidarreh, I. Akkurt, N. Almousa, H.M.H. Zakaly, Exploring the impact of sulfur-antimony incorporation on the radiation shielding, structural, physical, and electrical properties of $(S_3Sb_2)_x$ (S_2Ge) $100-x$ chalcogenide composites, J. Opt. Quantum Electron. 56 (2024) 1-16. https://doi.org/10.1007/s11082-024-06381-z.

[13] D.S. Baykal, G. Almisned, H. Alkarrani, H.O. Tekin, Radiation shielding characteristics and transmission factor values of some selected alloys: A monte carlo-based study, IJCESEN.10 (2024). https://doi.org/10.22399/ijcesen.421.

DOI: 10.62184/mmc.jmmc110020255

Research Article

[14] N. Tuncel, I. Akkurt, I. Atik, R.B. Malidarreh, M.I. Sayyed, Neutron-gamma shielding properties of chalcogenide glasses, J. Radiat. Phys. Chem. 218 (2024) 111582. https://doi.org/10.1016/j.radphyschem.2024.111582.

[15] A. Kumar, A. Kumar, R. Dogra, M. Manhas, S. Sharma, R. Kumar, Effect of gamma irradiation on thermoluminescence studies of LiF: Sm^{3+}, Dy^{3+} nanophosphor, J. Emerg. Mater. Res. 9 (2020) 122-131. https://doi.org/10.1680/jemmr.18.00101.

[16] M.I. Sayyed, Radiation shielding properties of aluminosilicate glass systems using PhyX software, *J. Adv. Res. Appl. Sci. Eng. Technol*. 37 (2024) 156-164. https://doi.org/10.37934/araset.37.2.156164.

[17] R.B. Malidarre, I. Akkurt, The influence of Nd_2O_3 on the radiation shielding, physical, mechanical, and acoustic properties of the (75 − x) TeO_2–15MgO–10Na_2O–xNd_2O_3 glasses as a potent radiation shielding material, J. Polym. Compos. 43 (2022) 5418–5425. https://doi.org/10.1002/pc.26844.

[18] G. ALMisned, E. Rabaa, D.S. Baykal, E. Ilik, G. Kilic, H.M.H. Zakaly, A. Ene, H.O. Tekin, The impact of chemical modifications on gamma-ray attenuation properties of some WO_3-reinforced tellurite glasses, Open Chem. 21(2023). https://doi.org/10.1515/chem-2022-0297.

[19] J.S. Alzahrani, Z.A. Alrowaili, A.V. Lebedev, I.O. Olarinoye, A. Hammoud, L.V. Vasileva, M.S. Al-Buriahi, Optical properties and radiation shielding performance of tellurite glassy composites: Role of rare earth oxides, J. Radiat. Phys. Chem. 212 (2023) 111168. https://doi.org/10.1016/j.radphyschem.2023.111168.

[20] S. Kabir, H. Ejaz, S.Z. Hussain, M.A. Rasheed, K. Junaid, A. Rehman, Effect of tellurite on growth of extensively drug resistant (XDR) *Mycobacterium tuberculosis* and action on mycobacterial drug efflux pump, J. King Saud Univ. Sci. 35(2023) 102629. https://doi.org/10.1016/j.jksus.2023.102629.

[21] A.A. Ahmed, F. Abbas, Optical absorption characteristics of Ni^{2+} in mixed-alkali borate glasses. J. Am. Ceram. Soc. 66 (1983) 434–439. https://doi.org/10.1111/j.1151-2916.1983.tb10076.x.

[22] K.M. Nutakki,G. Yerramreddy, N. Veeraiah, Role of nickel ion coordination on spectroscopic and dielectric properties of ZnF_2– As_2O_3–TeO_2: NiO glass system. J. Non-Cryst. Solids, 357 (2011) 1193– 1202. https://doi.org/10.1016/j.jnoncrysol.2010.11.016.

[23] D. Souri, A. Salehizahed, Effect of NiO content on the optical bandgap, refractive index, and density of TeO_2– V_2O_5–NiO glasses. J. Mater. Sci. 44 (2009) 5800–5805. https://doi.org/10.1007/s10853-009-3814-z .

[24] I. Akkurt, P.B. Malidarreh, R.B. Malidarre, Simulation, and prediction the attenuation behavior of the KNN-LMN based lead-free ceramics by FLUKA code and artificial neural network (ANN)-based algorithm, J. Environ. Technol. 44 (2022) 1-15. https://doi.org/10.1080/09593330.2021.2008017.

[25] H.O. Tekin, Gh. Almisned, G. Susoy, H.M.H. Zakaly, S.A.M. Issa, G. Kilic, Y.S. Rammah, G. Lakshminarayana, A. Ene, A detailed investigation on high-dense CuZr Bulk Metallic Glasses for shielding purposes, Open Chem. 20 (2022) 69-80. https://doi.org/10.1515/chem-2022-0127.

[26] H. Alkarrani, D.S. Baykal, G. ALMisned, H.O. Tekin, High-density lead germanate glasses with enhanced gamma and neutron shielding performance: impact of PbO concentration on attenuation properties, IJCESEN, 11 (2025) 1-9. https://doi.org/10.22399/ijcesen.635.

[27] S. Erdem, O.F. Ozpolat, B. Alım, M.I. Sayyed, M. Kurudirek, Phy-X / PSD: Development of a user friendly online software for calculation of parameters relevant to radiation shielding and dosimetry, J. Radiat. Phys. Chem. 166 (2020) 108496. https://doi.org/10.1016/j.radphyschem.2019.108496.

[28] M. Makishima, M.D. Mackenzie, Calculation of bulks modulus, shear modulus and Poisson's ratio of glass, J. Non-Cryst. Solids. 17 (1975) 147–157. https://doi.org/10.1016/0022-3093(75)90047-2.

[29] M. Makishima, M.D. Mackenzie, Direct calculation of Young's modulus of glass, J. Non-Cryst. Solids. 12 (1973) 35–45. https://doi.org/10.1016/0022-3093(73)90053-7.

[30] S. Inaba, S. Fujino, K. Morinaga, Young's modulus and compositional parameters of oxide glasses, J. Am. Ceram. Soc. 82 (1999) 3501–3507. https://doi.org/10.1111/j.1151-2916.1999.tb02272.x.

[31] F. Mezrag, N. Bouarissa, N.E. Fares, The elastic constants and related mechanical properties of AlxIn1−xP, J. Emerg. Mater. Res. 9 (2020) 1-6. http://dx.doi.org/10.1680/jemmr.20.00013.